UC Davis
UC Davis Previously Published Works

Title

Hydrogel mechanics are a key driver of bone formation by mesenchymal stromal cell spheroids

Permalink

https://escholarship.org/uc/item/2ck0b85w

Authors

Whitehead, Jacklyn
Griffin, Katherine H
Gionet-Gonzales, Marissa
et al.

Publication Date

2021-02-01

DOI

10.1016/j.biomaterials.2020.120607

Peer reviewed

Hydrogel Mechanics are a Key Driver of Bone Formation by Mesenchymal Stromal Cell Spheroids

Jacklyn Whitehead[1], **Katherine H. Griffin**[1,2], **Marissa Gionet-Gonzales**[1], **Charlotte E. Vorwald**[1], **Serena E. Cinque**[1], **J. Kent Leach**[1,3]

[1]Department of Biomedical Engineering, University of California, Davis, CA 95616

[2]School of Veterinary Medicine, University of California, Davis, CA 95616

[3]Department of Orthopaedic Surgery, UC Davis Health, Sacramento, CA 95817

Abstract

Mesenchymal stromal cells (MSCs) can promote tissue repair in regenerative medicine, and their therapeutic potential is further enhanced *via* spheroid formation. Stress relaxation of hydrogels has emerged as a potent stimulus to enhance MSC spreading and osteogenic differentiation, but the effect of hydrogel viscoelasticity on MSC spheroids has not been reported. Herein, we describe a materials-based approach to augment the osteogenic potential of entrapped MSC spheroids by leveraging the mechanical properties of alginate hydrogels. Compared to spheroids entrapped in covalently crosslinked elastic alginate, calcium deposition of MSC spheroids was consistently increased in ionically crosslinked, viscoelastic hydrogels. We previously demonstrated that intraspheroidal presentation of Bone Morphogenetic Protein-2 (BMP-2) on hydroxyapatite (HA) nanoparticles resulted in more spatially uniform MSC osteodifferentiation, providing a method to internally influence spheroid phenotype. In these studies, we observed significant increases in calcium deposition by MSC spheroids loaded with BMP-2-HA in viscoelastic gels compared to soluble BMP-2, which was greater than spheroids entrapped in all elastic alginate gels. Upon implantation in critically sized calvarial bone defects, bone formation was greater in all animals treated with viscoelastic hydrogels. Increases in bone formation were evident in viscoelastic gels,

---

CONFLICT OF INTEREST

The authors have no conflicts of interest.

Declaration of interests

The authors declare that they have no known competing financial interests or personal relationships that could have appeared to influence the work reported in this paper.

DATA AVAILABILITY STATEMENT

The raw/processed data required to reproduce these findings will be made available on request.

regardless of the mode of presentation of BMP-2 (*i.e.*, soluble delivery or HA nanoparticles). These studies demonstrate that the dynamic mechanical properties of viscoelastic alginate are an effective strategy to enhance the therapeutic potential of MSC spheroids for bone formation and repair.

Graphical Abstract

Keywords

mesenchymal stromal cells; spheroids; alginate; stress relaxation; bone regeneration

INTRODUCTION

Mesenchymal stromal cells (MSCs) are popular in cell-based therapies because of their accessibility from several tissue compartments, trophic factor secretion, and potential to differentiate toward numerous phenotypes.[1, 2] However, high rates of cell death upon transplantation have limited the effectiveness of such therapies,[3, 4] motivating the need for alternative approaches to utilize these multipotent cells. The therapeutic efficacy of MSCs can be increased through their formation into spheroids, three-dimensional aggregates of cells.[5, 6] Compared to monodisperse cells, spheroids exhibit improved cell survival, secrete increased concentrations of bioactive trophic factors, retain their multilineage potential, and represent a more physiologically relevant model of the native cell microenvironment.[7–9]

Osteoinductive cues such as Bone Morphogenetic Protein-2 (BMP-2) are potent stimuli to induce osteogenic differentiation of MSCs to bone-forming osteoblasts. However, soluble factors are insufficient to retain the desired cell phenotype upon the removal of these cues,[5, 10, 11] as occurs upon transplantation. We demonstrated that the incorporation of hydroxyapatite (HA) nanoparticles with adsorbed BMP-2 into spheroids increased MSC osteogenic potential.[12] Spheroids loaded with BMP-2-adsorbed HA exhibited more spatially uniform expression of osteoblastic markers throughout the aggregate versus soluble BMP-2, which induced expression of these markers that was limited primarily to the spheroid periphery.

The surrounding microenvironment can also influence cell phenotype, and numerous biomaterials have been studied to regulate cell function.[13] When used as a cell carrier, alginate can promote bone formation by entrapped cells due to its tunability to regulate adhesivity and substrate stiffness, along with minimally inflammatory characteristics.[14,

15] More recently, alginate was used to demonstrate the importance of viscoelasticity in a cell carrier on cell spreading[16, 17] and osteogenic differentiation.[18] Viscoelasticity allows entrapped cells to better engage and remodel the gel, similar to their behavior in the native extracellular matrix.[18–20] However, the role of substrate elasticity on the behavior of entrapped MSC spheroids has not been examined.

In this study, we demonstrate that the dynamic mechanical properties of viscoelastic alginate can promote the osteogenic potential of entrapped MSC spheroids. We combined an internal osteoinductive stimulus, provided by BMP-2-HA nanoparticles, with an external stimulus, alginate possessing distinct mechanical characteristics (*i.e.*, viscoelastic or elastic), to regulate the osteogenic phenotype of entrapped MSC spheroids. We then examined the capacity of MSC spheroids to promote bone formation in critically sized calvarial defects. These data show, for the first time, that MSC spheroid behavior is dependent upon the mechanical properties of the cell carrier to guide tissue engineering strategies for intramembranous bone formation.

MATERIALS AND METHODS

Cell culture

Human bone marrow-derived MSCs from a 22 year old male donor (Texas A&M Institute for Regenerative Medicine, Temple, TX) were received at passage 2. We confirmed the trilineage potential of these cells as an indicator of their multipotency prior to use. MSCs were expanded in standard culture conditions (37°C, 21% O_2, 5% CO_2) in α-MEM (Life Technologies, Carlsbad, CA) supplemented with 10% fetal bovine serum (FBS, Atlanta Biologicals, Flowery Branch, GA) and 1% penicillin/streptomycin (P/S, Gemini Bio Products, Sacramento, CA) until use at passage 4–5.

Spheroid formation

Spheroids were formed using a forced aggregation method.[12, 21] Briefly, MSCs (4.35×10^5 cells/mL) were pipetted into agarose molds in well plates, and the plates were centrifuged at $500 \times g$ for 8 min. Plates were maintained statically in standard culture conditions for 48 h to form spheroids. Each microwell contained 15,000 MSCs.

Human recombinant BMP-2 (Medtronic, Minneapolis, MN) was adsorbed onto 0.1 mg/mL of HA nanoparticles (100 nm average diameter, Berkeley Advanced Biomaterials, Berkeley, CA) by resuspending HA in phosphate buffered saline (PBS, Thermo Fisher Scientific, Waltham, MA) as previously described.[12] In brief, BMP-2 was added to a final concentration of 200 ng/mL in low adhesion conical tubes. After 90 min, the tubes were centrifuged at $500 \times g$ for 8 min, and the supernatant was aspirated, leaving the pelleted HA. The pellet was washed once with PBS, the mixture centrifuged again at $500 \times g$ for 8 min, and PBS was aspirated. The remaining pellet was resuspended in cell culture media for subsequent incorporation into spheroids. Approximately 50 ng/mL of BMP-2 was adsorbed onto the mass of HA nanoparticles.[12]

HA was incorporated into spheroid cultures by resuspending the cell pellet of known cell number in media containing HA. The HA-cell mixture was pipetted up and down for 5 s to

ensure homogeneity. The HA-cell suspension was then dispersed into the agarose molds and spheroids were formed as described above. Approximately 1 ng BMP-2 was presented from 3 ng HA in each spheroid.

For spheroids with soluble BMP-2 added (Sol BMP), spheroids were formed as described above except BMP-2 was not adsorbed to the HA. 50 ng/mL of BMP-2 was incorporated into the alginate hydrogel during formation.

Alginate hydrogel formation

Arginine-Glycine-Aspartic acid (RGD)-modified alginate was prepared as described.[6, 22, 23] Briefly, G_4RGDSP (Commonwealth Biotechnologies, Richmond, VA) was covalently coupled to UltraPure MVG (200,000 ± 8,700 g/mol) and VLVG sodium alginate (32,000 ± 200 g/mol), both from Pronova, Lysaker, Norway) using standard carbodiimide chemistry, yielding hydrogels with a degree of substitution of 2. Degree of substitution is defined as the number of peptide ligands conjugated to a single alginate polymer chain, corresponding to a bulk RGD density of 0.8 mM for these gels. The molecular weight of both alginates was measured using Triple Detection Size Exclusion Chromatography (SEC)/Gel Permeation Chromatography (GPC) Analysis (PolyAnalytik Inc., Los Angeles, CA). The resulting RGD-alginate was sterile filtered and lyophilized for 4 days.

Lyophilized alginate was reconstituted in PBS for ionically crosslinked alginate or in 2-(N-morpholino)ethanesulfonic acid hydrate (MES) buffer for covalently crosslinked alginate to obtain a 2.1% (w/v) solution. MSC spheroids were then entrapped in alginate and either ionically crosslinked with 50 mg/mL calcium carbonate ($CaCO_3$) and 200 mg/mL of D-glucono-δ-lactone (GDL) and 200 mM $CaCl_2$ or covalently crosslinked with 75 mM of dihydrazide (AAD)/1-hydroxybenzotriazole (HOBT) with 100 mg/mL of 1-ethyl-3-(dimethylaminopropyl) carbodiimide (EDC) (all from Sigma-Aldrich, St. Louis, MO) (Table 1). The reagents were mixed for 30 s using a 2-way stopcock to thoroughly blend all solutions with the cell suspension. The gel was cast between parallel glass plates with 1 mm thickness and incubated for 3 h at 37 °C. Hydrogel disks were produced with an 8 mm biopsy punch and placed in α-MEM with 10% FBS.

Characterization of alginate hydrogel mechanical properties

The viscoelastic properties of alginate gels were measured using a Discovery HR2 Hybrid Rheometer (TA Instruments, New Castle, DE). An 8.0 mm-diameter Peltier plate geometry was used for hydrogels with a corresponding 8.0 mm diameter. An oscillatory strain sweep ranging from 0.004% to 4% strain was performed on each gel to obtain the linear viscoelastic region (LVR) before gel failure. At least 6 data points were collected for the LVR and averaged to obtain gel shear storage modulus after initial formation.[14] Frequencies and strain levels used for rheology are specific to laboratory protocols, as previously described,[14] and these protocols also yield the storage modulus, loss modulus, and tan delta. The viscoelastic properties of alginate hydrogels were measured after 1 and 7 days in culture medium. Stress relaxation of alginate hydrogels was measured using an Instron 3345 Compressive Testing System (Norwood, MA).[18] Hydrogels were loaded between two flat platens and compressed at 0.05 mm/sec for 18 s, then the top platen was

held at a constant 10% strain for 132 s, for a total testing time of 2.5 min. Stress relaxation time was calculated by determining the time for the initial stress of the material to relax to half of the original value ($\tau_{1/2}$).[18] To determine mass loss, hydrogels were weighed after 1 day in media for wet weight, frozen overnight at −80 °C, lyophilized for two days, and then weighed again to denote the initial, Day 1 dry weight. A corresponding set of hydrogels were kept in culture medium for 7 days, with the media changed every other day, then frozen at −80 °C overnight, lyophilized for two days, and weighed to denote the dry weight over time.

Spheroid characterization

MSCs were maintained in osteogenic media consisting of α-MEM supplemented with 50 μg/mL ascorbate-2-phosphate, 10 mM β-glycerophosphate, and 100 nM dexamethasone (all from Sigma-Aldrich) for 12 days in monolayer culture. These MSCs were then trypsinized and formed into spheroids using the forced aggregation method. Spheroid formation progressed over 48 h in osteogenic media for a total of 14 days of osteoinduction.[12, 24] To collect spheroids from alginate hydrogels for analysis, hydrogels were minced with a razor blade and then sonicated for 20 s in passive lysis buffer (Promega, Madison, WI). DNA content was determined using the Quant-iT PicoGreen DNA Assay Kit (Invitrogen, Carlsbad, CA), intracellular alkaline phosphatase (ALP) activity was measured as previously described,[25] and calcium deposition was quantified using a Stanbio™ Calcium Liquid Reagent kit (Thermo Fisher). All values are presented after subtracting initial calcium levels from acellular gels and accounting for HA as a calcium source. Osteocalcin (OCN) secretion was measured with protein-specific ELISA kits per the manufacturer's instructions (R&D Systems, Minneapolis, MN). Cell viability was evaluated by a Live/Dead assay (Life Technologies), and representative images were assessed with ImageJ. We quantified the viability of these spheroids using three images from each group. We ascertained the area of the green mask (live cells) versus the total area of the spheroid (green and red masks merged). This difference was then expressed as a percent of live cells. To study cell interaction with the hydrogel, alginate was first modified with GGGGRGDASSK (CSBio, Menlo Park, CA) or the scrambled control peptide GGGGRDGASSK (Genscript, Piscataway, NJ). Alginate was then fluorescently labeled after peptide modification using an amine reactive dye (Thermo Fisher Scientific, Waltham, MA) as previously described.[24] Aspect ratio was determined *via* Imaris 9.6 (Abingdon, United Kingdom) software by using the create surface function for the spheroid and hydrogel, from which we calculated the width over height for the resulting crater from the corresponding 3D image.

Evaluation of cytoskeletal structure of MSCs entrapped in alginate

At day 7 of culture, gels were fixed with 4% paraformaldehyde at 4°C overnight, washed twice with PBS, and permeabilized with 0.05% Triton-X 100 for 5 min at room temperature. Gels were stained with Alexa Fluor 488 Phalloidin solution (Thermo Fisher; 1:40 in PBS) and incubated at room temperature for 1 h. Gels were washed once with PBS and stained with DAPI (Thermo Fisher; 1:500 in PBS) at room temperature for 10 min. Gels were washed twice with PBS and subsequently imaged using confocal microscopy (Leica TCS SP8, Wetzlar, Germany) at 40X magnification.

Assessment of implant osteogenic potential *in vivo*

Before implantation, osteogenically induced MSCs were stained with 10 μM of the near infrared (NIR) dye CellBrite NIR680 Cytoplasmic Membrane Dye (Biotium, Fremont, CA) per manufacturer's instructions. In brief, MSCs were resuspended at 1×10^6 in warmed culture medium containing the desired concentration of NIR dye. This cell suspension was incubated for 20 min at 37°C, protected from light. Cells wer e then pelleted at $500\times g$ for 8 min. The supernatant was removed, and cells were washed a total of 3 times in warm medium. MSCs were aggregated into spheroids as described above. The NIR signal was detected using an *In Vivo* Imaging System (IVIS) Spectrum (Perkin Elmer, Waltham, MA) for fluorescence imaging (emission wavelength of 675 nm, excitation wavelength of 740 nm). Images were quantified using the IVIS's accompanying software.

Animals were treated in accordance with all University of California, Davis animal care guidelines and National Institutes of Health (NIH) animal handling procedures. Male and female athymic rats (NIH/RNU, 10 weeks old, Taconic) were anesthetized and maintained under a 1–3% isoflurane/O_2 mixture delivered through a nose cone. 8 mm critically sized defects were surgically created in the calvaria using a trephine burr (ACE Surgical Supply, Brockton, MA). Defects were immediately filled with MSC spheroids containing BMP-2-adsorbed HA nanoparticles entrapped in viscoelastic alginate (Viscoelastic BMP HA) or elastic alginate (Elastic BMP HA). As a control group, an equal dose of soluble BMP-2 was mixed into viscoelastic alginate gels containing HA-loaded MSC spheroids (Viscoelastic Sol BMP). The incision was closed with sutures and/or wound clips and buprenorphine (0.05 mg/kg) was administered twice per day for two days as analgesia.

Quantification of bone formation

Two weeks post-implantation, constructs were collected, imaged for detection of NIR signal, fixed in 10% formalin for 24 h, demineralized in Calci-Clear Rapid (National Diagnostics, Atlanta, GA), processed, paraffin-embedded, and sectioned at 5 μm. Sections were stained with hematoxylin and eosin (H&E) and imaged using a Nikon Eclipse TE2000U microscope and Andor Zyla 5.5 sCMOS digital camera (Concord, MA). In order to visualize transplanted human cells undergoing osteogenic differentiation, sections underwent immunohistochemistry (IHC) using a primary antibody against DLX5 (AF6710, 1:20, R&D Systems, Minneapolis, MN), an early marker for BMP-responsive transcriptional activator needed for osteoblast differentiation.[26, 27]

At 12 weeks post-implantation, all remaining animals were euthanized, and calvariae were explanted, fixed in 10% formalin for 24 h, and transferred to 70% ethanol. Constructs were imaged (70 kVp, 114 μA, 300 ms integration time, average of three images) at 15 μm resolution using a high resolution microcomputed tomography (microCT) specimen scanner (μCT 35; Scanco Medical, Brüttisellen, Switzerland). Bone volume fraction (BVF) and bone mineral density (BMD) were determined from resulting images using the accompanying software. Explants were then demineralized in Calci-Clear Rapid (National Diagnostics), processed, paraffin-embedded, and sectioned at 5 μm thickness. Sections were stained with Masson's Trichrome.

Statistical analysis

Data are presented as means ± standard deviation, and all *in vitro* data represent a minimum of 3 independent experiments. Statistical analysis was performed using a one-way analysis of variance (ANOVA) with a Tukey's multiple comparison *post hoc* test. All statistical analyses were performed using Prism 8 software (GraphPad, San Diego, CA); *p* values less than 0.05 were considered statistically significant. Significance is denoted by alphabetical letterings. Groups with statistically significant differences do not share the same letters; ns denotes no significance among all groups.

RESULTS

Mechanical properties of alginate hydrogels are tunable

We investigated the tunability of stress relaxation in alginate hydrogels immediately after formation and over time. Though the molecular weights (MVG and VLVG) and crosslinking agents (ionic and covalent) were varied between groups, alginate hydrogels were morphologically comparable, with covalent hydrogels appearing slightly clearer while the ionic gels were opaquer due to entrapped calcium carbonate (Fig. 1A). The wet and dry mass of viscoelastic hydrogels after 1 day in culture was lower compared to elastic gels (Supplemental Fig. 1A and 1B), and gels composed only of VLVG demonstrated the largest swelling ratios after 1 day in culture (Supplemental Fig. 1C). After 7 days in culture, VLVG viscoelastic gels had the lowest wet and dry mass (Supplemental Fig. 1E and 1F), but there were no statistically significant differences in swelling ratios among all groups (Supplemental Fig. 1D).

We measured the storage and loss modulus to interrogate the elastic and viscous components of our hydrogels. The storage modulus measures the stiffness of the material by quantifying the elastic energy stored within the gel. All alginate hydrogels exhibited comparable storage moduli after 1 day in culture, with VLVG gels exhibiting slightly lower moduli than gels containing MVG (p 0.003) (Fig. 1B). The loss modulus alternatively quantifies the viscoelastic component, or the energy dissipated from the hydrogel. We found the loss modulus of viscoelastic gels after 1 day in culture was higher than elastic gels (p 0.0002) (Fig. 1C), and elastic gels demonstrated the lowest tan delta after 1 day in culture ($p < 0.0001$) (Supplemental Fig. 2A). Hydrogel viscoelasticity was characterized by stress relaxation time, the time for the viscoelastic materials to relax to half of their initial value ($\tau_{1/2}$), which was tunable based on alginate molecular weight and crosslinking agent (Fig. 1D). Viscoelastic VLVG alginate exhibited the fastest stress relaxation time, ~20 s (p 0.002) (Fig. 1E). As expected, covalently crosslinked alginate did not exhibit stress deformation under constant strain, and $\tau_{1/2}$ could not be calculated. Storage and loss moduli after 7 days in media (Fig. 1F and 1G), as well as the tan delta (Supplemental Fig. 2B), followed similar trends as initial moduli. The stress relaxation characteristics of viscoelastic alginates were retained over time, and elastic alginate did not relax (Fig. 1H). When quantified, $\tau_{1/2}$ decreased in all viscoelastic groups except VLVG, which remained similar to initial values (Fig. 1I). These data indicate that we successfully synthesized alginate hydrogels with tunable stress relaxation properties through varying the molecular weight and crosslinking agent. We selected one elastic and one viscoelastic group for further study,

namely VLVG covalently crosslinked alginate and VLVG ionically crosslinked alginate, respectively. These groups were chosen because they exhibited significant differences in loss moduli and stress relaxation characteristics while displaying no differences in swelling ratio or initial storage moduli.

Osteogenic potential of MSC spheroids is increased in viscoelastic gels

We next interrogated the effect of viscoelastic and elastic alginate hydrogels on the osteogenic potential of entrapped MSCs (Fig. 2A). We did not detect differences in DNA content, an indicator of cell number, when MSCs were entrapped as monodisperse cells or spheroids after 14 days (p 0.376) (Fig. 2B). After 14 days in osteogenic media, MSCs in viscoelastic alginate, whether monodisperse or spheroids, exhibited increased calcium deposition compared to cells in elastic gels (p 0.026) (Fig. 2C).

Having replicated the established phenomenon that monodisperse MSCs exhibit greater osteogenic potential when entrapped in viscoelastic alginate compared to elastic gels [18], the remainder of our studies used MSC spheroids to elucidate the effect of viscoelastic alginate on entrapped cellular aggregates (Fig. 2D). The osteogenic potential of MSC spheroids was increased when HA-loaded MSC spheroids were entrapped in viscoelastic gels (Fig. 2E and 2F). MSC spheroids containing BMP-2-HA nanoparticles demonstrated the greatest calcium deposition when entrapped in viscoelastic VLVG alginate (p 0.001) and the greatest ALP activity when entrapped in elastic or viscoelastic VLVG alginate (p 0.022) compared to MSC spheroids with BMP-2 and HA in other configurations. All viscoelastic groups outperformed their elastic counterparts.

To investigate the mechanism of how viscoelasticity enhances the osteogenic potential of BMP-2-HA loaded MSC spheroids, we evaluated the degree to which MSC spheroids interacted with their environment. Specifically, we investigated how MSC spheroids bind and remodel viscoelastic versus elastic hydrogels, and how this influences their osteogenic differentiation. First, to interrogate the influence of cell interaction and stress relaxation, we entrapped spheroids in alginate modified with either fluorescently tagged RGD, a cell adhesive peptide, or fluorescently tagged scrambled RDG, a non-adhesive control (Fig. 3A). MSC spheroids entrapped in RGD-modified viscoelastic hydrogels exhibited significantly higher calcium production compared to cells in elastic RGD-modified hydrogels ($p=0.0006$), indicating the combination of viscoelasticity and RGD enhances osteogenic differentiation. However, spheroids entrapped in RDG-modified gels demonstrated comparable calcium production in both viscoelastic and elastic hydrogels ($p=0.991$), confirming the importance of cell engagement and mechanosensing their surroundings through interaction with RGD (Fig. 3B). When imaged by confocal microscopy, spheroids in all groups appeared similar, with slightly more elongations and extensions in RGD-modified gels (Fig. 3C). As an indicator of engagement with the hydrogel, we quantified the aspect ratio of the crater, or indentation, resulting from spheroids entrapped in the hydrogel. Viscoelastic RGD groups trended towards the highest aspect ratio values compared to elastic and scrambled groups (Fig. 3D). These findings suggest that cell-matrix adhesion through RGD and stress relaxation enable more cell engagement with the material.

To further interrogate cellular function within our platform, we used a ROCK inhibitor, Y-27632, to abrogate cytoskeletal activity within MSCs and restrict MSC remodeling of the alginate matrix. These studies were initially conducted with HA-loaded spheroids lacking BMP-2 to focus on the effect of MSCs within a viscoelastic versus elastic hydrogel environment (Fig. 3E). We observed decreased calcium deposition in ROCK-inhibited spheroids in viscoelastic gels compared to untreated controls ($p<0.0001$), providing further evidence that MSC interaction with a viscoelastic substrate enhances osteogenic differentiation (Fig. 3F). It should also be noted that knockdown of ROCK activity can have negative effects on cell-ECM activity within the spheroid, resulting in stunted MSC function. Therefore, we focused on visualizing the cells on the periphery of the spheroid, those that would exhibit the highest interaction with the alginate, through confocal imaging. When BMP-2 was delivered to MSCs on HA nanoparticles, we observed faint phalloidin staining for cells in viscoelastic hydrogels compared to elastic gels (Fig. 3H). Smaller actin fibers are characteristic of cells seeded in viscoelastic hydrogels compared to elastic substrates, which could explain this observation.[28] Additionally, MSCs undergoing late stages of osteogenic differentiation may be less likely to migrate.[29] Actin signal in all groups was reduced upon addition of Y-27632, verifying that inhibiting the ROCK pathway decreases stress fiber and focal adhesion formation as previously reported.[30] We did not observe significant differences in the aspect ratio of entrapped MSC spheroids, an indicator of spheroid remodeling of the gel, suggesting that differences in actin expression do not correlate with cell spreading or migration in this system (Fig. 3I). From these data, we conclude that although BMP-HA spheroids appear to be interacting with their matrix through RGD in a way that enhances their osteogenic potential, this does not manifest into significant cell migration or actin formation. Overall, these data indicate that BMP-HA MSC spheroids sense stress relaxation through both binding and remodeling their matrix, thus allowing them to enhance their osteogenic potential in viscoelastic hydrogels.

Having established the influence of substrate mechanics and internal osteoinductive stimuli on MSC spheroid function *in vitro*, we carried forward three MSC spheroid-containing gels that demonstrated the greatest osteogenic potential (Viscoelastic BMP HA, Elastic BMP HA, and Viscoelastic HA Sol BMP) to the translational component of our study. The aforementioned gels were implanted into a critically sized rat calvarial defect, and a parallel study was performed *in vitro* to compare the translational potential of our groups. After two weeks, we examined the viability and osteogenic potential of MSC spheroids *in vitro* and *in vivo*. Spheroid viability was high in all groups (Fig. 4A). The percentage of live cells was comparable in elastic alginate (85.3%) to cells in both viscoelastic gels (90.3% and 90.0%) (p 0.549) (Fig. 4B). Calcium deposition by MSCs entrapped in viscoelastic gels was higher than elastic gels (Fig. 4C). Interestingly, osteocalcin (OCN) secretion was greatest in MSC spheroids containing HA nanoparticles with soluble BMP treatment (p 0.033) (Fig. 4D). The results from our *in vitro* characterizations were verified *in vivo* with punctated DLX5 staining, an early marker for osteogenic differentiation, throughout the neotissue in all groups (Fig. 4E).

We used near infrared (NIR) imaging to verify that MSC spheroids remained viable in implanted hydrogels *in vivo* two weeks after implantation. Upon explantation, MSC spheroids were visible in all calvariae, regardless of experimental group (Fig. 5A). The NIR

signal was lower when MSCs were implanted in elastic hydrogels, yet no statistical differences were observed between groups (p 0.129) (Fig. 5B). Alginate hydrogels began to dissociate after two weeks *in vivo*, as evidenced by the presence of alginate fragments in the histological sections (Fig. 5C).

After 12 weeks, we observed significant differences in calcified tissue formation within treated defects using microCT (Fig. 6A). Defects treated with MSC spheroids entrapped in viscoelastic alginate exhibited enhanced bone volume compared to those treated with elastic alginate. However, there was no significant difference in bone volume for defects treated with MSC spheroids in viscoelastic alginate, regardless of osteoinductive stimulus (p 0.379) (Fig. 6B). We observed similar trends for bone mineral density (Fig. 6C). These trends were also consistent when bone volume and bone mineral density were analyzed as a function of sex (Supplemental Fig. 3). Interestingly, defects in male rats treated with MSC spheroids with BMP-2-HA nanoparticles entrapped in viscoelastic alginate outperformed all other groups (Supplemental Fig. 3A and 3C), yet bone volume and bone mineral density between sexes was not statistically different (Supplemental Fig. 3B and 3D). Masson's Trichrome revealed the presence of new bone formation on the edge of all defects, yet osteoid was only observed in the center of defects treated with Viscoelastic BMP HA (Fig. 6D).

DISCUSSION

Despite improved cell-cell and cell-matrix communication compared to monodispersed cells, MSC spheroids may benefit from additional instructional cues to promote their direct participation in tissue formation. In this study, we demonstrate that the dynamic mechanical properties of viscoelastic alginate can enhance *in situ* differentiation and promote the osteogenic phenotype of entrapped MSC spheroids. This work demonstrates the influence of stress relaxation in alginate hydrogels on the osteogenic potential of MSC spheroids. Several recent studies have reinforced the effect of substrate viscoelasticity on cell biology, namely increased cell spreading proliferation, and osteogenic differentiation.[18] However, the majority of these studies have examined the response of monodisperse cells within engineered hydrogels. Compared to monodisperse cells, we and others have demonstrated the improved therapeutic potential of MSC spheroids that possess increased survival, trophic factor secretion, and differentiation potential.[23, 31–33] In light of the promising synergy between cell spheroids and substrate viscoelasticity, this study evaluated the instructive capacity of stress relaxation on the osteogenic potential of entrapped MSC spheroids.

The stress relaxation and initial mechanical properties of alginate hydrogels are dependent upon the polymer molecular weight, type and density of crosslinking agent, and gelation protocols.[18] The interplay between cellular response and alginate mechanics has been studied under numerous conditions. For example, fibroblasts embedded in alginate gels with variable densities of polyethylene glycol (PEG) to achieve distinct stress relaxation characteristics demonstrated increased cell spreading and proliferation in gels with faster stress relaxation.[34] In this study, we used an ionic crosslinking agent, $CaCO_3$, to form viscoelastic alginate and a covalent crosslinking agent, AAD, to form elastic alginate. $CaCO_3$ is a commonly used source of divalent cations to crosslink alginate. However, since

it is used as a supersaturated solution, hydrogels can contain entrapped undissolved particles of $CaCO_3$ and gas bubbles, resulting in issues with hydrogel uniformity. We mixed the hydrogel vigorously using a luer lock system to combat this issue, yet viscoelastic groups still exhibited larger variation in elastic moduli compared to elastic groups. Importantly, these groups exhibited significantly different stress relaxation times while possessing similar elastic moduli. Chemistries used for covalent crosslinking have been implicated in unintended and potentially adverse effects on entrapped cells. [15, 35] In these studies, we observed only a slight reduction in the viability of MSC spheroids in the elastic hydrogel group after two weeks. Therefore, spheroid viability is likely not responsible for the observed differences in *in vivo* outcomes.

The influence of hydrogel stress relaxation on cell behavior has been widely reported for entrapped monodisperse cells that interact extensively with the polymer matrix.[3, 4] In contrast, only the cells on the periphery of a spheroid directly interact with the hydrogel matrix, presenting a vastly different physical and chemical environment to entrapped cells. This motivates the need to further study the effects of dynamic mechanical properties on entrapped spheroids. MSC spheroids exhibited limited cell spreading and corresponding tension on cytoskeletal fibers when entrapped in viscoelastic alginate. These results are in contrast to our previous findings that an RGD degree of substitution (DS) of 2 is sufficient to promote osteogenically induced MSC migration from spheroids entrapped in viscoelastic alginate.[14] However, the previously reported studies used MSCs that were osteogenically induced as spheroids, enabling the accumulation of endogenous ECM within the spheroid, while we induced cells in monolayer before spheroid formation and incorporating BMP-2 adsorbed HA nanoparticles. MSCs at later stages of osteogenic differentiation can exhibit slower migration with greater adhesivity.[29] Our previous studies demonstrate that simultaneous delivery of osteoinductive signals (BMP-2 and HA) enhanced markers of osteogenic differentiation in MSC spheroids.[12] Osteogenically induced MSC spheroids containing BMP-2-adsorbed HA may be differentiated to a more advanced stage of osteogenesis, resulting in an inhibition of their chemotactic response to substrate-mediated cues. Alginate hydrogels modified with higher RGD concentrations (DS=10) enhanced cell spreading of monodisperse osteogenically induced MSCs in viscoelastic alginate.[36] Thus, integrin engagement within the DS 2 hydrogel matrix may be insufficient to stimulate cell spreading of MSC spheroids at the time point we investigated. The role of RGD concentration on the migration and osteogenic potential of BMP-2-HA containing MSC spheroids warrants further investigation.

Although we observed little to no migration of MSCs from the spheroid, interactions between the hydrogel and cells occurred, evidenced by the decrease in calcium deposition when MSC spheroids in viscoelastic gels were treated with Y-27632 or entrapped in nonadhesive RDG-modified hydrogels. Our data suggest that MSCs engage the biomaterial, and these interactions are a contributing factor to enhance osteogenic differentiation of MSC spheroids. Additionally, the fraction of cells that could actively migrate out of the spheroid represents a small percentage of the overall cell density in the gels. Therefore, markers for the holistic behavior of the entrapped spheroids are more informative. Spheroids entrapped in viscoelastic alginate demonstrated enhanced calcium deposition and ALP activity, both markers of the osteogenic phenotype.

This study unites several established elements in the pursuit of effective bone formation. Stress relaxation is an important stimulus to guide the proliferation and differentiation of monodisperse cells, and its impact has been confirmed using numerous polymeric systems. [18, 34, 37, 38] However, compared to monodisperse cells in alginate gels, these studies are more physiologically relevant due to the increased cell-cell and cell-extracellular matrix interactions that occur within 3D cell aggregates. The importance of the interplay between substrate characteristics and cell behavior within dense, 3D tissue culture has been underscored in recent studies focused on cancer progression. For example, aggregates of mammary epithelial cells will assume malignant phenotypes when matrix stiffness is increased.[39] Our studies used human MSCs in spheroid form, which behave distinctly different than cancer cell aggregates.[40]

These data establish, for the first time, the effect of stress relaxation on the osteogenic potential of MSC spheroids. Consistent with findings using monodisperse MSCs, our data demonstrate that the osteogenic potential of MSC spheroids is enhanced when entrapped in viscoelastic gels. After 12 weeks *in vivo*, we observed significantly more bone tissue formation in defects treated with spheroids in viscoelastic alginate, regardless of the presence of the BMP-2. The accumulation of calcified material in the defect is due to an absolute regeneration of bone, evidenced by a net increase in calcified material compared to the initial mass of HA incorporated into the spheroids. Similar quantities of HA were added in both viscoelastic and elastic alginate hydrogels, yet we detected little calcified material in elastic hydrogels after 12 weeks. There was no measurable difference in calcified material between groups containing spheroids with BMP-2 HA nanoparticles or when soluble BMP-2 was added to the hydrogel. Thus, the instructive biomaterial, rather than the internal stimulus of BMP-2, increased the osteogenic potential of entrapped MSC spheroids to a greater degree.

CONCLUSION

These studies demonstrate that the dynamic mechanical properties of viscoelastic alginate, achieved *via* ionic crosslinking, enhance the therapeutic potential of MSC spheroids for bone formation and repair. For the first time, we provide evidence that the stress relaxation characteristics of viscoelastic alginate are retained over time and can be used for regenerative therapies using MSC spheroids. Thus, BMP-2-adsorbed HA nanoparticles incorporated into MSC spheroids, in synergy with entrapment in a viscoelastic alginate hydrogel, show great promise for cell-based therapies to promote bone formation.

Supplementary Material

Refer to Web version on PubMed Central for supplementary material.

ACKNOWLEDGEMENTS

REFERENCES

[1]. Caplan AI, Correa D, The MSC: an injury drugstore, Cell Stem Cell 9(1) (2011) 11–15. [PubMed: 21726829]

[2]. Grayson WL, Bunnell BA, Martin E, Frazier T, Hung BP, Gimble JM, Stromal cells and stem cells in clinical bone regeneration, Nat Rev Endocrinol 11(3) (2015) 140–50. [PubMed: 25560703]

[3]. Eggenhofer E, Luk F, Dahlke MH, Hoogduijn MJ, The life and fate of mesenchymal stem cells, Front Immunol 5 (2014) 148. [PubMed: 24904568]

[4]. Moya A, Paquet J, Deschepper M, Larochette N, Oudina K, Denoeud C, Bensidhoum M, Logeart-Avramoglou D, Petite H, Human mesenchymal stem cell failure to adapt to glucose shortage and rapidly use intracellular energy reserves through glycolysis explains poor cell survival after implantation, Stem Cells 36(3) (2018) 363–376. [PubMed: 29266629]

[5]. Murphy KC, Hoch AI, Harvestine JN, Zhou D, Leach JK, Mesenchymal stem cell spheroids retain osteogenic phenotype through α2β1 signaling, Stem Cell Transl Med 5(9) (2016) 1229–1237.

[6]. Ho SS, Murphy KC, Binder BY, Vissers CB, Leach JK, Increased survival and function of mesenchymal stem cell spheroids entrapped in instructive alginate hydrogels, Stem Cells Transl Med 5(6) (2016) 773–81. [PubMed: 27057004]

[7]. Xu Y, Shi TP, Xu AX, Zhang L, 3D spheroid culture enhances survival and therapeutic capacities of MSCs injected into ischemic kidney, J Cell Mol Med 20(7) (2016) 1203–1213. [PubMed: 26914637]

[8]. Petrenko Y, Sykova E, Kubinova S, The therapeutic potential of three-dimensional multipotent mesenchymal stromal cell spheroids, Stem Cell Res Ther 8(1) (2017) 94. [PubMed: 28446248]

[9]. Vorwald CE, Joshee S, Leach JK, Spatial localization of endothelial cells in heterotypic spheroids influences Notch signaling, J Mol Med 98(3) (2020) 425–435. [PubMed: 32020237]

[10]. Hoch AI, Mittal V, Mitra D, Vollmer N, Zikry CA, Leach JK, Cell-secreted matrices perpetuate the bone-forming phenotype of differentiated mesenchymal stem cells, Biomaterials 74 (2016) 178–187. [PubMed: 26457835]

[11]. Law S, Chaudhuri S, Mesenchymal stem cell and regenerative medicine: regeneration versus immunomodulatory challenges, Am J Stem Cells 2(1) (2013) 22–38. [PubMed: 23671814]

[12]. Whitehead J, Kothambawala A, Leach JK, Morphogen Delivery by Osteoconductive Nanoparticles Instructs Stromal Cell Spheroid Phenotype, Adv Biosyst 3(12) (2019) 1900141. [PubMed: 32270027]

[13]. Gonzalez-Fernandez T, Sikorski P, Leach JK, Bio-instructive materials for musculoskeletal regeneration, Acta Biomater 96 (2019) 20–34. [PubMed: 31302298]

[14]. Ho SS, Keown AT, Addison B, Leach JK, Cell migration and bone formation from mesenchymal stem cell spheroids in alginate hydrogels are regulated by adhesive ligand density, Biomacromolecules 18(12) (2017) 4331–4340. [PubMed: 29131587]

[15]. Lee KY, Mooney DJ, Alginate: properties and biomedical applications, Prog Polym Sci 37(1) (2012) 106–126. [PubMed: 22125349]

[16]. Chaudhuri O, Gu L, Darnell M, Klumpers D, Bencherif SA, Weaver JC, Huebsch N, Mooney DJ, Substrate stress relaxation regulates cell spreading, Nat Commun 6(1) (2015) 1–7.

[17]. Grolman JM, Weinand P, Mooney DJ, Extracellular matrix plasticity as a driver of cell spreading, Proc Natl Acad Sci U.S.A 117(42) (2020) 25999–26007. [PubMed: 33020289]

[18]. Chaudhuri O, Gu L, Klumpers D, Darnell M, Bencherif SA, Weaver JC, Huebsch N, Lee HP, Lippens E, Duda GN, Mooney DJ, Hydrogels with tunable stress relaxation regulate stem cell fate and activity, Nat Mater 15(3) (2016) 326–34. [PubMed: 26618884]

[19]. DuFort CC, Paszek MJ, Weaver VM, Balancing forces: architectural control of mechanotransduction, Nat Rev Mol Cell Biol 12(5) (2011) 308–19. [PubMed: 21508987]

[20]. Zhao X, Huebsch N, Mooney DJ, Suo Z, Stress-relaxation behavior in gels with ionic and covalent crosslinks, J Appl Phys 107(6) (2010) 63509. [PubMed: 21464912]

[21]. Vorwald CE, Ho SS, Whitehead J, Leach JK, High-throughput formation of mesenchymal stem cell spheroids and entrapment in alginate hydrogels, Biomaterials for Tissue Engineering: Methods and Protocols 1758 (2018) 139–149.

[22]. Rowley JA, Madlambayan G, Mooney DJ, Alginate hydrogels as synthetic extracellular matrix materials, Biomaterials 20(1) (1999) 45–53. [PubMed: 9916770]

[23]. Ho SS, Hung BP, Heyrani N, Lee MA, Leach JK, Hypoxic preconditioning of mesenchymal stem cells with subsequent spheroid formation accelerates repair of segmental bone defects, Stem Cells 36(9) (2018) 1393–1403. [PubMed: 29968952]

[24]. Hoch AI, Mittal V, Mitra D, Vollmer N, Zikry CA, Leach JK, Cell-secreted matrices perpetuate the bone-forming phenotype of differentiated mesenchymal stem cells, Biomaterials 74 (2016) 178–87. [PubMed: 26457835]

[25]. Hoch AI, Binder BY, Genetos DC, Leach JK, Differentiation-dependent secretion of proangiogenic factors by mesenchymal stem cells, PLoS One 7(4) (2012) e35579. [PubMed: 22536411]

[26]. Samee N, Geoffroy V, Marty C, Schiltz C, Vieux-Rochas M, Levi G, de Vernejoul MC, Dlx5, a positive regulator of osteoblastogenesis, is essential for osteoblast-osteoclast coupling, Am J Pathol 173(3) (2008) 773–780. [PubMed: 18669617]

[27]. Harvestine JN, Gonzalez-Fernandez T, Sebastian A, Hum NR, Genetos DC, Loots GG, Leach JK, Osteogenic preconditioning in perfusion bioreactors improves vascularization and bone formation by human bone marrow aspirates, Sci Adv 6(7) (2020) eaay2387. [PubMed: 32095526]

[28]. Marozasabc IA, Anseth KS, Cooper-White JJ, Adaptable boronate ester hydrogels with tunable viscoelastic spectra to probe timescale dependent mechanotransduction, Biomaterials 223 (2019) 1800638.

[29]. Ichida M, Yui Y, Yoshioka K, Tanaka T, Wakamatsu T, Yoshikawa H, Itoh K, Changes in cell migration of mesenchymal cells during osteogenic differentiation, FEBS Lett 585(24) (2011) 4018–24. [PubMed: 22100295]

[30]. Amano M, Nakayama M, M KKA, Rho-kinase/ROCK: A key regulator of the cytoskeleton and cell polarity, Cytoskeleton (Hoboken, N.J.) 67(9) (2010) 545–554.

[31]. Bartosh TJ, Ylöstalo JH, Mohammadipoor A, Bazhanov N, Coble K, Claypool K, Lee RH, Choi H, Prockop DJ, Aggregation of human mesenchymal stromal cells (MSCs) into 3D spheroids enhances their antiinflammatory properties, Proc Natl Acad Sci U S A 107(31) (2010) 13724–9. [PubMed: 20643923]

[32]. Murphy KC, Fang SY, Leach JK, Human mesenchymal stem cell spheroids in fibrin hydrogels exhibit improved cell survival and potential for bone healing, Cell Tissue Res 357(1) (2014) 91–9. [PubMed: 24781147]

[33]. Baraniak PR, McDevitt TC, Scaffold-free culture of mesenchymal stem cell spheroids in suspension preserves multilineage potential, Cell Tissue Res 347(3) (2012) 701–11. [PubMed: 21833761]

[34]. Nam S, Stowers R, Lou J, Xia Y, Chaudhuri O, Varying PEG density to control stress relaxation in alginate-PEG hydrogels for 3D cell culture studies, Biomaterials 200 (2019) 15–24. [PubMed: 30743050]

[35]. Smeds KA, Pfister-Serres A, Miki D, Dastgheib K, Inoue M, Hatchell DL, Grinstaff MW, Photocrosslinkable polysaccharides for in situ hydrogel formation, J Biomed Mater Res 54(1) (2001) 115–21. [PubMed: 11077410]

[36]. Chaudhuri O, Gu L, Darnell M, Klumpers D, Bencherif SA, Weaver JC, Huebsch N, Mooney DJ, Substrate stress relaxation regulates cell spreading, Nat Commun 6 (2015) 6364.

[37]. Sülo lu AK, Karacao lu E, Bilgic HA, Selmano lu G, Koçkaya EA, Karaaslan C, Osteogenic differentiation of adipose tissue-derived mesenchymal stem cells on fibrin glue- or fibronectin-coated Ceraform®, J Biomater Appl 34(3) (2019) 375–385. [PubMed: 31165664]

[38]. Hesse E, Hefferan TE, Tarara JE, Haasper C, Meller R, Krettek C, Lu L, Yaszemski MJ, Collagen type I hydrogel allows migration, proliferation, and osteogenic differentiation of rat bone marrow stromal cells, J Biomed Mater Res A 94(2) (2010) 442–449. [PubMed: 20186733]

[39]. Chaudhuri O, Koshy ST, Branco da Cunha C, Shin JW, Verbeke CS, Allison KH, Mooney DJ, Extracellular matrix stiffness and composition jointly regulate the induction of malignant phenotypes in mammary epithelium, Nat Mater 13(10) (2014) 970–8. [PubMed: 24930031]

[40]. Lee JY, Chang JK, Dominguez AA, Lee HP, Nam S, Chang J, Varma S, Qi LS, West RB, Chaudhuri O, YAP-independent mechanotransduction drives breast cancer progression, Nat Commun 10(1) (2019) 1848. [PubMed: 31015465]
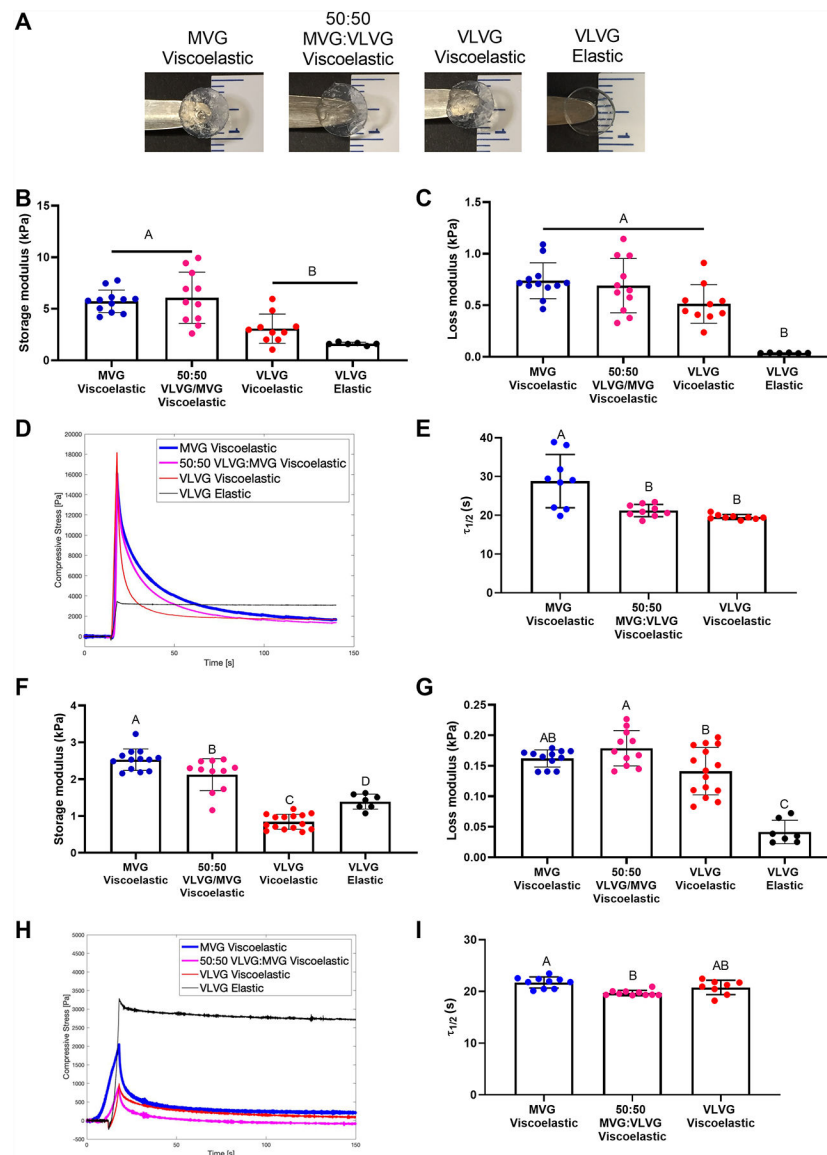
Figure 1. Hydrogel stress relaxation is dictated by alginate molecular weight and crosslinking agent.

(**A**) Representative images of alginate hydrogels immediately after formation. (**B**) Shear storage modulus after 1 day in culture medium as a function of molecular weight and crosslinking agent (n=6–12). (**C**) Loss modulus after 1 day in culture medium as a function of molecular weight and crosslinking agent (n=6–12). (**D**) Representative image of the deformation of compressive stress over time as a function of crosslinking agent and alginate molecular weight. (**E**) Quantification of stress relaxation time ($\tau_{1/2}$) for ionically crosslinked alginate as a function of molecular weight (n=9). (**F**) Shear storage modulus after 7 days in culture medium as a function of molecular weight and crosslinking agent (n=7–15). (**G**) Loss modulus after 7 days in culture medium as a function of molecular weight and crosslinking agent (n=7–15). (**H**) Representative image of the deformation of compressive stress over time as a function of crosslinking agent and alginate molecular weight after 5 days in cell culture medium. (**I**) Quantification of the stress relaxation time for alginate

crosslinked with an ionic crosslinking agent as a function of molecular weight after 7 days in cell culture medium (n=8–10). Significance is denoted by alphabetical letterings. Groups with statistically significant differences do not share the same letters; ns denotes no significance among all groups.
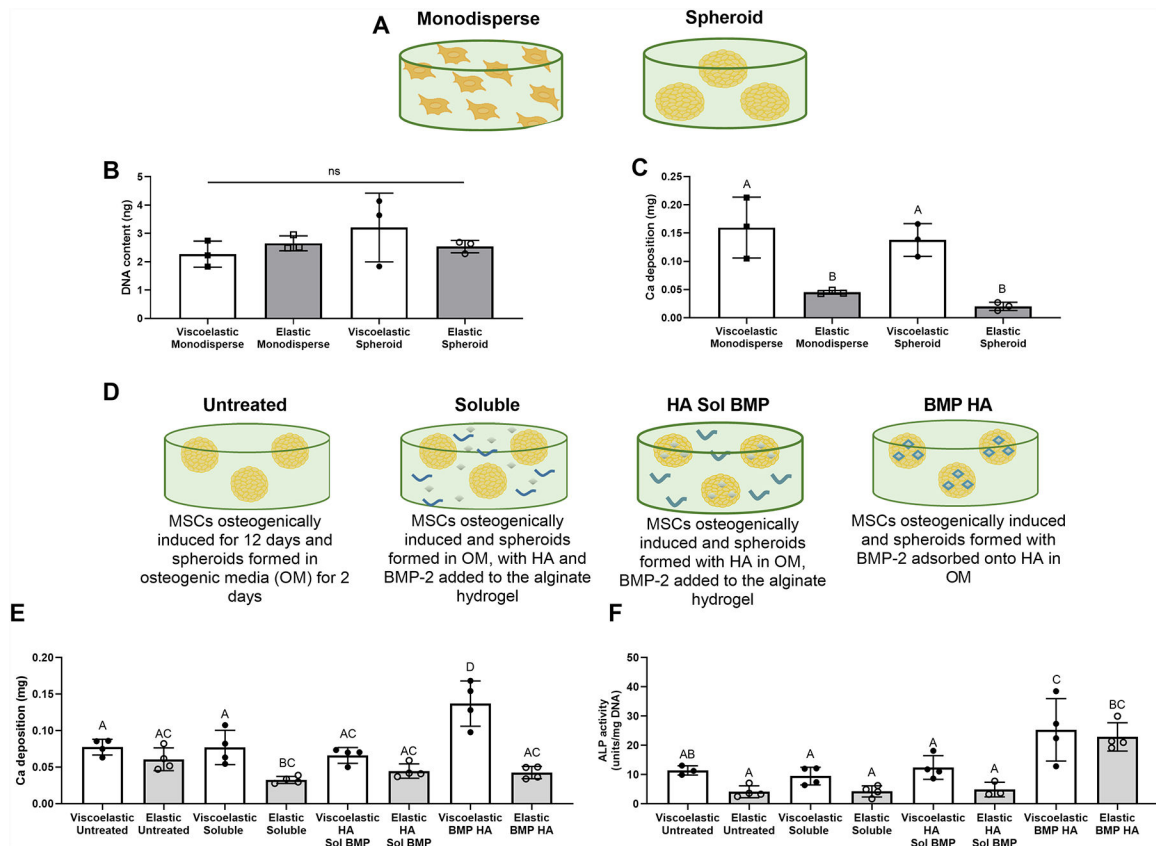
Figure 2. The osteogenic potential of MSC spheroids is enhanced in viscoelastic alginate.
(**A**) Schematic depicting the use of MSCs in data presented in **B** and **C**. (**B**) DNA content of MSCs entrapped in viscoelastic and elastic VLVG alginate as monodisperse cells or spheroids (n=3). (**C**) Calcium deposition in gels loaded with monodisperse cells or MSC spheroids (n=3). (**D**) Schematic depicting the use of internal cues in **E**. (**E**) Calcium deposition in gels containing MSC spheroids after 14 days as a function of stimulus (n=4). (**F**) ALP activity in gels containing MSC spheroids after 5 days (n=3–4). Significance is denoted by alphabetical letterings. Groups with statistically significant differences do not share the same letters; "ns" denotes no significance among all groups.
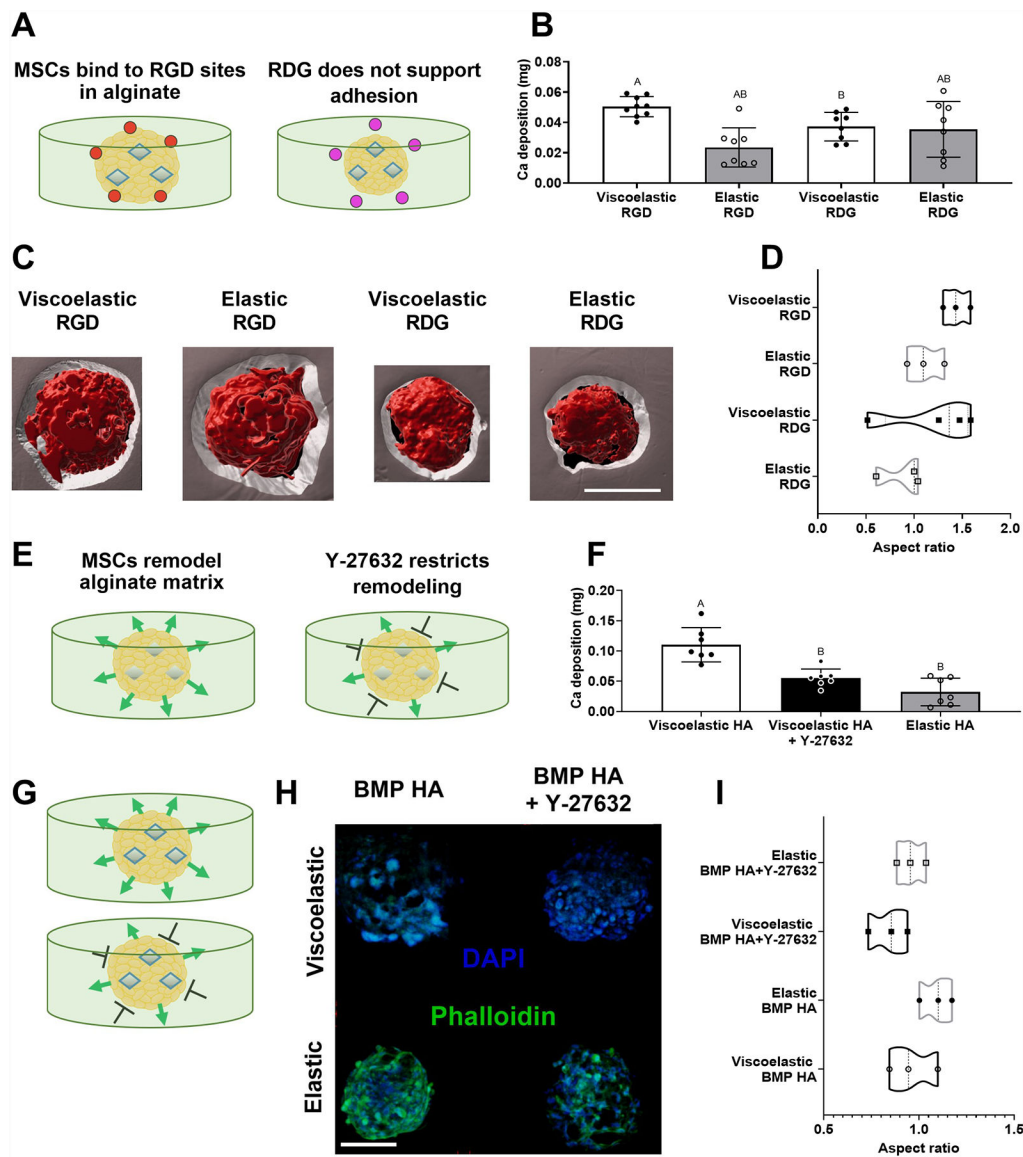
Figure 3. MSC spheroids sense properties of viscoelastic alginate through RGD adhesion and ROCK signaling for resultant osteogenic response.
(**A**) Schematic representing the potential influence of adhesion ligands for MSC spheroids in alginate hydrogels. (**B**) Calcium deposition within gels containing MSC spheroids after 10 days as a function of viscoelasticity and adhesion peptide (n=8–9). (**C**) Representative 3D rendering following processing of confocal images of MSC spheroids (red) in RGD- or RDG-modified alginate (grey) after 14 days in culture. Scale bar is 100 μm. (**D**) Aspect ratio quantified from void volumes created by spheroids entrapped in the hydrogel after 14 days (n=3). Schematic representing the hypothesized influence of adding Y-27632 to alginate hydrogels with spheroids loaded with (**E**) HA (**G**) or BMP HA. (**F**) Calcium deposition within gels containing MSC spheroids treated with Y-27632 as a function of viscoelasticity after 14 days (n=7). (**H**) Representative confocal images of MSC spheroids stained with DAPI (blue) and phalloidin (green) after 7 days in culture. Scale bar is 200 μm. (**I**) Aspect ratio calculated for MSC spheroids in elastic and viscoelastic hydrogels treated with or

without Y-27632 after 7 days (n=3). Significance is denoted by alphabetical letterings. Groups with statistically significant differences do not share the same letters.
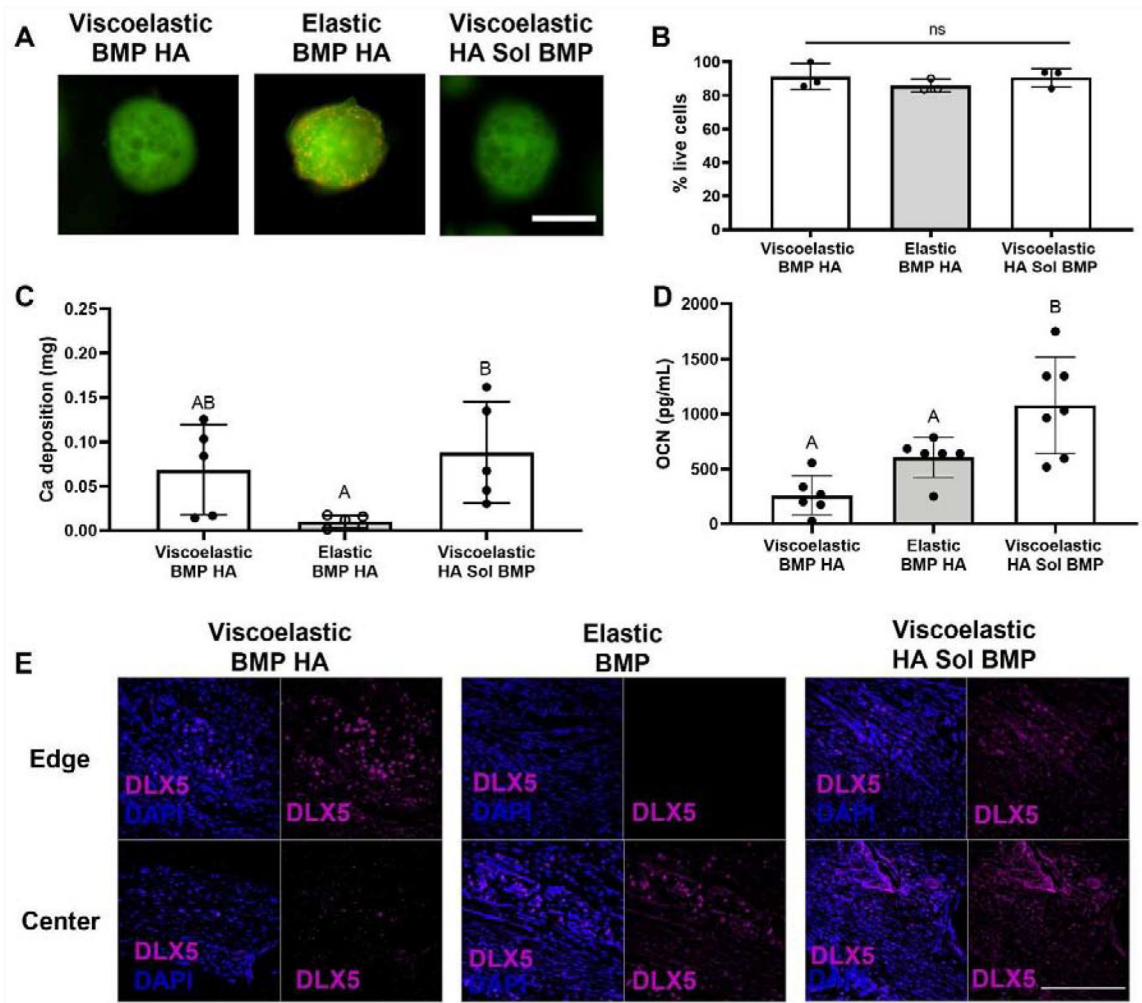
Figure 4. The viability and osteogenic potential of MSC spheroids is enhanced in viscoelastic alginate.

(**A**) Representative images of spheroids after 14 days in culture. Live cells are green and red cells are dead. Scale bar is 500 μm. (**B**) Quantification of live cells after 14 days in culture (n=3) (**C**) Calcium accumulation within viscoelastic and elastic alginate hydrogels over 14 days (n=5). (**D**) Cell-secreted osteocalcin after 14 days in culture (n=6–7). Significance is denoted by alphabetical letterings. Groups with statistically significant differences do not share the same letters. (**E**) Representative images of DLX5 staining (magenta) counterstained with DAPI (blue) from edge or center of the calvarial defect. Scale bar is 200 μm.
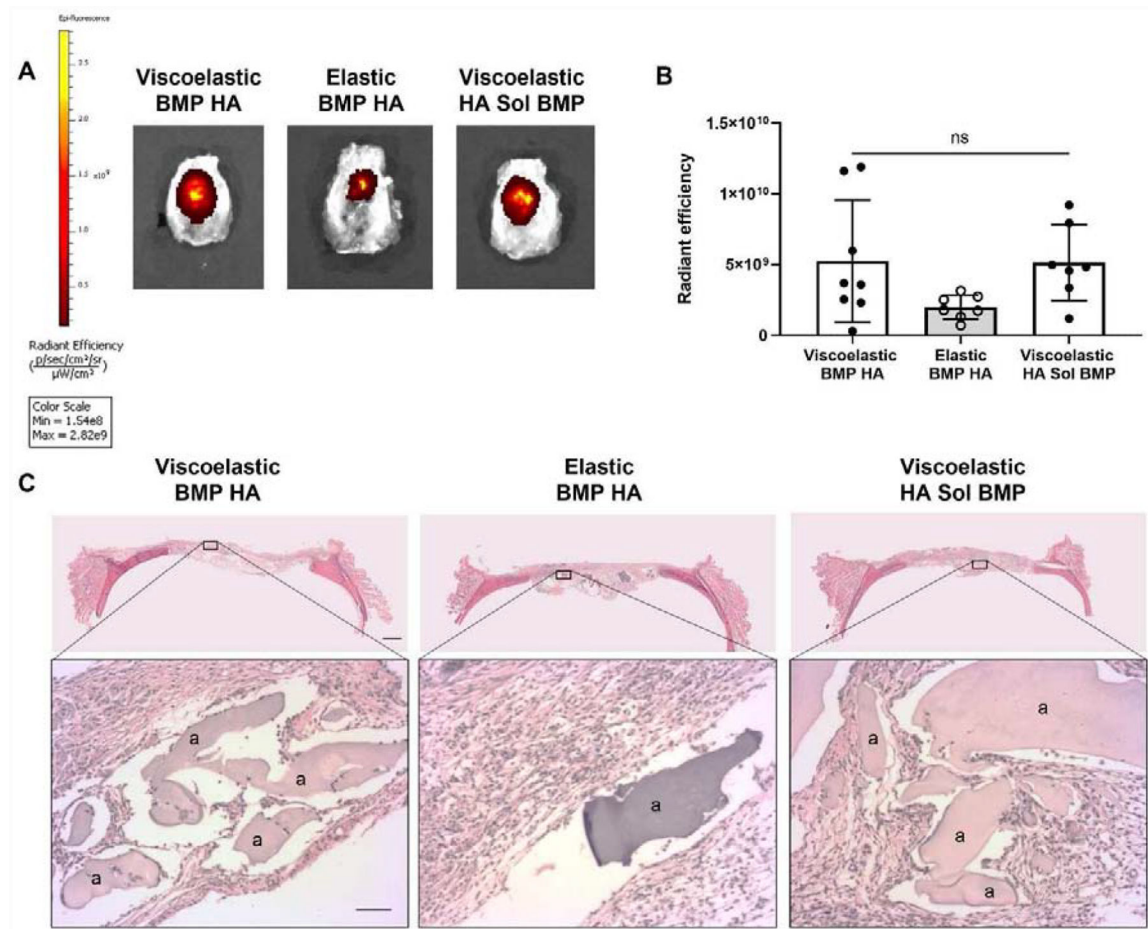
Figure 5. MSC spheroids persist *in vivo*.
(**A**) Representative images of explanted rat calvariae 2 weeks post-implantation exhibit NIR signal localized to the defect site. (**B**) Quantification of the NIR signal in each experimental group. Significance is denoted by alphabetical letterings; ns denotes no significance among all groups (n=7–8). (**C**) Representative images of H&E staining of calvarial defects from each group. Top images are large scans of an entire cross-section of the defect. Scale bar is 1 mm. The bottom insert images are 10X magnified regions of interest. The "a" denotes alginate. Bottom scale bar is 200 μm.
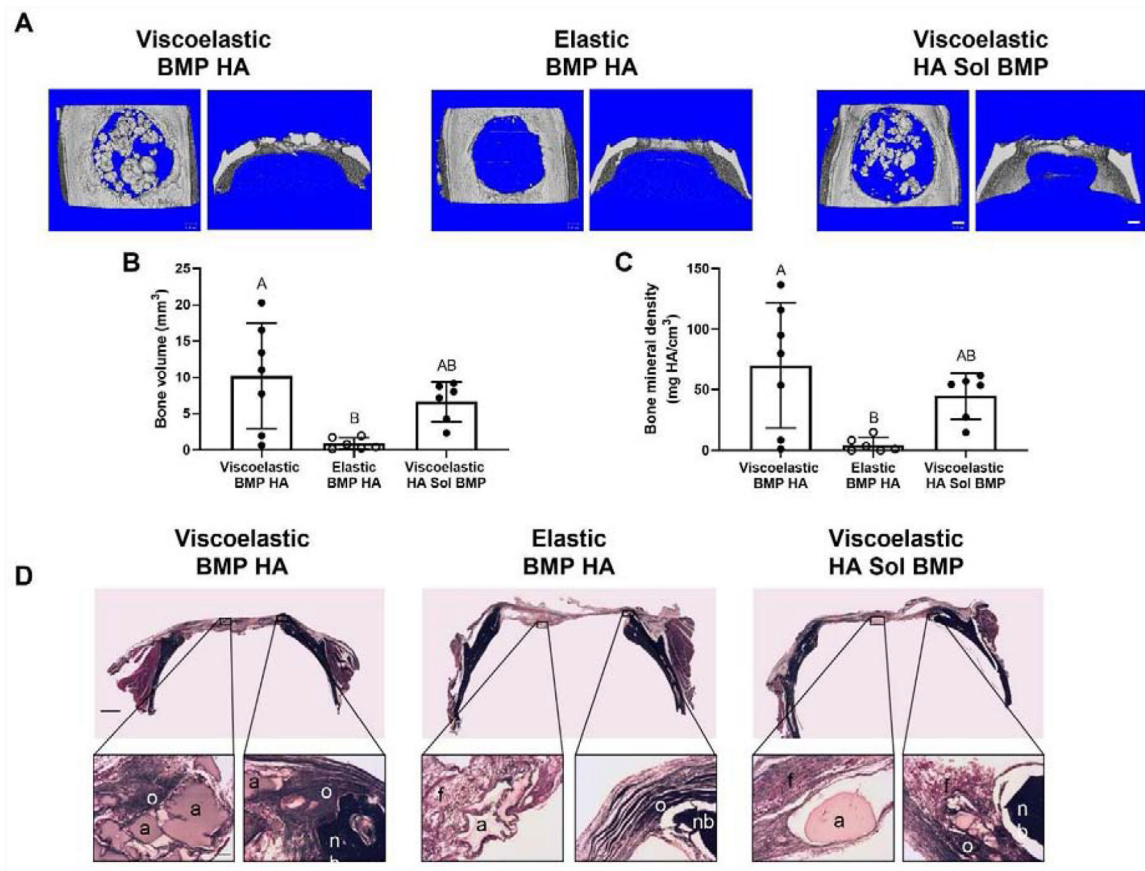
Figure 6. MSC spheroids promote bone tissue formation *in vivo* when entrapped in viscoelastic alginate.

(**A**) Representative images of microCT scans of explanted rat calvariae 12 weeks after hydrogel implantation. Scale bars are 1 mm. (**B**) Bone volume (n=6–7). (**C**) Bone mineral density (n=6–7). Significance is denoted by alphabetical letterings. Groups with statistically significant differences do not share the same letters. (**D**) Representative images of Masson's Trichrome staining of calvarial defects from each group. Top images are large scans of an entire cross-section of the defect. Scale bar is 1 mm. The bottom insert images are 10X magnified regions of interest on either the center (left) or edge (right) of the defect. Residual alginate: a; fibrous tissue: f; native bone: nb; osteoid: o. Bottom scale bar is 200 μm.

Table 1.

List of hydrogel compositions used in these studies

Description	% Alginate	Alginate Weight Average	Resuspension Solution	Crosslinking Agent	Crosslinking Additive
Ionically crosslinked MVG	2%	200,000 ± 8,700 g/mol	PBS	50 mg/mL CaCO$_3$	200 mg/mL GDL
Ionically crosslinked VLVG:MVG	2%	32,000 ± 200 to 200,000 ± 8,700 g/mol	PBS	50 mg/mL CaCO$_3$	200 mg/mL GDL
Ionically crosslinked VLVG	2%	32,000 ± 200 g/mol	PBS	50 mg/mL CaCO$_3$	200 mg/mL GDL
Covalently crosslinked VLVG	2%	32,000 ± 200 g/mol	MES buffer	75 mM AAD/HOBT	100 mg/mL EDC